Atmos. Meas. Tech. Discuss., 7, 1457–1493, 2014
www.atmos-meas-tech-discuss.net/7/1457/2014/
doi:10.5194/amtd-7-1457-2014

Atmospheric Measurement Techniques
Discussions
Open Access

# Retrieval of tropospheric column-averaged $CH_4$ mole fraction by solar absorption FTIR-spectrometry using $N_2O$ as a proxy

**Z. Wang[1], N. M. Deutscher[1,2], T. Warneke[1], J. Notholt[1], B. Dils[3], D. W. T. Griffith[2], M. Schmidt[4], M. Ramonet[4], and C. Gerbig[5]**

[1]Institute of Environmental Physics, University of Bremen, Germany
[2]School of Chemistry, University of Wollongong, Wollongong, Australia
[3]Belgian Institute for Space Aeronomy, Brussels, Belgium
[4]Laboratoire des Sciences du Climat et de l'Environnement (LSCE), Gif-Sur-Yvette, France
[5]Max-Plank-Institute für Biogeochemie, Jena, Germany

Received: 30 December 2013 – Accepted: 31 January 2014 – Published: 13 February 2014

Correspondence to: Z. Wang (zhiting@iup.physik.uni-bremen.de)

Published by Copernicus Publications on behalf of the European Geosciences Union.

## Abstract

Tropospheric column-averaged $CH_4$ mole fractions were derived from ground-based absorption columns measurements. The method used stratospheric $N_2O$ columns to correct for the stratospheric contribution to the $CH_4$ total column. The method was applied to four TCCON sites covering locations from the Northern Arctic to the tropics. It performs well for all sites. The derived tropospheric $CH_4$ concentrations were compared with profiles measured by aircraft at three sites. The results indicate an inter-site consistency within 6 ppb (∼ 0.3 %). With aircraft profiles up to 3 km, the seasonal behavior of the derived tropospheric $CH_4$ concentration was also checked. It reveals a difference of 20 ppb around. The mean relative uncertainty of the four sites is 0.23 %. Comparing with the method using HF the proposed method shows a smaller relative uncertainty and less $H_2O$ dependence.

## 1 Introduction

Methane ($CH_4$) is the second most important anthropogenic greenhouse gas in the atmosphere (Montzka et al., 2011). The main sources of $CH_4$ to the atmosphere are natural wetlands, anthropogenic activities (livestock production; rice cultivation; production, storage, transmission, and distribution of fossil fuels; waste waters and landfills) and biomass burning. The destruction by OH in the troposphere is the dominant atmospheric sink of $CH_4$. Both anthropogenic and natural emissions of $CH_4$ are likely to increase in the twenty-first century as global population increases and climate warms. The atmospheric mole fraction of methane has increased from about 700 ppb to the current atmospheric background of about 1800 ppb since 1770. Despite this dramatic increase, the observed global annual mean atmospheric abundance was nearly constant from 1999 to 2006, before it began to increase again in 2007 (Rigby et al., 2008; Dlugokencky et al., 2009). This behaviour is a subject of open scientific discussion (Bousquet et al., 2011; Pison et al., 2013).

Atmospheric $CH_4$ concentrations measurements can be linked quantitatively to regional sources and sinks by inverse modeling. Improving both the quality and quantity of measurements is a way to better constrain source and sinks, since it is an underconstrained problem. The Total Carbon Column Observation Network (TCCON) was founded to remotely measure column abundances of $CO_2$, $CH_4$, CO, $N_2O$ and other molecules that absorb in the near infrared (NIR) (Wunch et al., 2011). The Network for the Detection of Atmospheric Composition Change (NDACC) ground-based solar absorption spectrometry in mid infrared (MIR) spectral regions can provide total column measurement for many gases (Sussmann et al., 2013). Such column data are essential for the validation of greenhouse gas measurements from satellites and as input or independent validation for inverse model studies. The column-averaged dry-air mole fraction (DMF) of $CH_4$ (known as $X_{CH_4}$) can be determined by ratioing to the retrieved column of the reference gas $O_2$, whose atmospheric abundance is well known. The tropospheric column-averaged mole fraction of $CH_4$ can be derived using methods based on: (i) a posteriori correction using a proxy for variations in the stratospheric contribution to the total column, such as the HF total column as an estimator for the stratospheric $CH_4$ contribution (Washenfelder et al., 2003; Warneke et al., 2006); and (ii) direct determination of the tropospheric mole fraction of $CH_4$ via retrieval of $CH_4$ profiles (Sepúlveda et al., 2012). Currently the second method is only applied to NDACC high-resolution MIR solar absorption spectra, not to the NIR TCCON spectra. The first method is based on the fact that HF is solely present in the stratosphere and a linear relationship exists between the DMFs of the $CH_4$ and HF with respect to changes in tropopause height. The stratospheric column of the $CH_4$ can therefore be inferred from the total column of the HF via this linear relationship, and then subtracted from the total column of the $CH_4$ to yield the tropospheric $CH_4$ column. Variations in the $CH_4$ column due to changes in surface pressure are determined from the $O_2$ column. Using this method, the tropospheric column-averaged DMF of $CH_4$ can be determined with a precision of 0.5 % (Washenfelder et al., 2003).

In stratosphere, a compact correlation exists between species of sufficiently long lifetime (Plumb et al., 1992). Species whose local lifetimes are longer than quasi-horizontal transport time scales share surfaces of constant mixing ratio, and a scatter plot of the mixing ratio of one vs. that of the other collapses to a compact curve. These correlations have been demonstrated by datasets from both chemical transport model and in situ measurements, such as observations taken from an aircraft platform (Avallone et al., 1997), ATMOS observations (Michelson et al., 1998) and balloon observations (Herman et al., 1998). This is true in the case of $CH_4$ and $N_2O$ in the stratosphere. Hence, using $N_2O$ to infer the stratospheric contribution of the total column of the $CH_4$ is an alternative approach, which is however complicated by the fact that $N_2O$ is also present in the troposphere. In this work, we describe a method to derive the tropospheric column-averaged DMF of $CH_4$ in which the stratospheric $N_2O$ column is used to estimate the stratospheric column of the $CH_4$. We apply the method to TCCON spectra at four sites, one tropical, two extra-tropical and one polar, and compare it with the results derived with the method using HF. In the following Sect. 2 introduce measurements site and data. Section 3 describes the method, while Sect. 4 presents the results and discussion. In Sect. 5 we give an uncertainty analysis and summarize the merits of our proposed method in Sect. 6.

## 2 Measurements site and data analysis

### 2.1 FTIR data

Here we use solar absorption Fourier-Transform (FT) measurements at four TCCON stations Ny-Ålesund (78.9° N, 11.9° E) at Spitsbergen (Palm et al., 2010), Orléans (47.97° N, 2.113° E) in France, Bialystok (53.23° N, 23.025° E) in Poland (Messerschmidt et al., 2010, 2012), and Darwin (12.424° S, 130.892° E) in Australia (Deutscher et al., 2010). The observations in the near infrared cover the spectral range between 4000 cm$^{-1}$ and 10 000 cm$^{-1}$ and were carried out with a $CaF_2$ beamsplitter and a room-temperature InGaAs photodiode.

The spectra were analyzed using the non-linear least-squares spectral fitting algorithm code GFIT, developed at NASA/JPL (Toon et al., 1992). Atmospheric absorption coefficients are calculated line-by-line for each gas in a chosen spectral window, and for each retrieval level using the assumed temperature, pressure and a priori DMF profile in the forward model. All these absorption coefficients together produce the atmospheric transmittance spectrum. The temperature, pressure and water vapor profiles are obtained from National Centers for Environmental Prediction (NCEP) reanalysis data provided by the NOAA/ESRL Physical Sciences Division (Kalnay et al., 1996), and interpolated in time and space from six hourly data to local solar noon and site latitude/longitude. The simulated spectrum is compared with the measured spectrum and DMF profiles are iteratively scaled to minimize the least-squares differences between the calculated and measured spectra. The measured spectra are solar radiation added by absorption feature of atmospheric gases. The spectral regions used in this study are the TCCON-standard regions given in Wunch et al. (2010).

## 2.2 In situ measurements

To validate the tropospheric $CH_4$ derived from FTIR measurements, in situ data from several sources are used. At Ny-Ålesund (78.9° N, 11.9° E) in situ $CH_4$ data are available from NOAA surface flask measurements (Dlugokencky et al., 2012) measured at Zeppelin mountain. Its elevation is 474 m a.s.l. There are low aircraft flight data available at Orléans, which have been taken two times every month since 1998 and up to 3 km, corresponding to 700 hPa in pressure coordinate. Over Bialystok there is regular profiling with semi-monthly to monthly observations using flask sampling at multiple levels up to 3 km for $CO_2$, $CH_4$, $N_2O$ and other tracers since 2002. These measurements are extended into the whole atmosphere by applying a linear interpolation between 3.0 km and the tropopause altitude and assuming the GFIT a priori above tropopausse. The tropospheric column-averaged $CH_4$ abundances obtained are used to check the seasonal behavior of the FTIR tropospheric column-averaged $CH_4$ mole fraction.

In addition, data from the HIPPO and IMECC aircraft campaigns are used to calibrate the derived tropospheric column-averaged $CH_4$ mole fractions. The HIAPER Pole-to-Pole Observations (HIPPO) of Carbon Cycle and Greenhouse Gases Study measures cross sections of atmospheric concentrations approximately pole-to-pole, from the surface to the tropopause (Wofsy et al., 2011). A comprehensive suite of atmospheric trace gases pertinent to understanding the Carbon Cycle were measured. The measurements are taken using the High-performance instrumented Airborne Platform for Environmental Research (HIAPER). In this work, the measurements near the TCCON site at Darwin are used. The IMECC project aimed to build the infrastructure for a coordinated, calibrated, integrated and accessible dataset for characterizing the carbon balance of the European. The aircraft campaign conducted within the IMECC project was organized by the Max Planck Institute for Biogeochemistry. Learjet 35 aircraft was equipped with a cavity ringdown spectroscopy instrument (Picarro Inc.) for $CO_2$ and $CH_4$ mixing ratio measurements and with a vacuum UV fluorescence analyzer for mixing ratio measurements of CO. Profiles were taken from 300 m to 12 000 m over the European TCCON stations including Bialystok and Orléans during September and October in 2009 (Geibel et al., 2012).

## 3 Method

For both HF and $N_2O$, assuming there is a linear relationship between their stratospheric mole fractions, $x$, and that of the $CH_4$ in the stratosphere, then

$$x_{CH_4}(z) = a + b \cdot x_y(z) \tag{1}$$

where, $y$ represents HF or $N_2O$. Figure 1 presents the correlation of the stratospheric mole fractions of HF (left) and $N_2O$ (right) with $CH_4$ based on retrievals from the ACE-FTS satellite (Bernath et al., 2005). For the derivation of *a* and *b*, the retrieved stratospheric profiles of HF, $N_2O$ and $CH_4$ are separated into several 20° wide latitude bands. In case of HF, the latitudinal variation of the slope *b* ranges from 740 ~ 870 $\mathrm{ppb\,ppb^{-1}}$, and from 3.6 to 4.4 $\mathrm{ppb\,ppb^{-1}}$ for $N_2O$. Between 2004 and 2010 no discernable time-dependency could be detected. For the four TCCON sites: Spitsbergen, Bialystok, Orléans and Darwin their corresponding slopes *b* for their corresponding latitude bands are 4.34, 4.39, 4.39 and 3.53 respectively for $N_2O$, and −749.05, −751.21, −751.21 and −876.03 for HF.

Here, we employ two strategies to retrieve the tropospheric column-averaged $CH_4$ mole fraction. Each one is described below: one strategy explicitly uses tropopause pressure to correct for the contribution of stratospheric $CH_4$ and the other one relies on the variation of HF or $N_2O$ to implicitly derive the tropopause height.

### 3.1 Strategy explicitly using tropopause pressure

Multiplying both sides of Eq. (1) with air density and integrating it over the stratosphere yields,

$$\mathrm{VC}_{\mathrm{CH_4}}^{\mathrm{strat}} = a \cdot \mathrm{VC}_{\mathrm{air}}^{\mathrm{strat}} + b \cdot \mathrm{VC}_{y}^{\mathrm{strat}} \tag{2}$$

where VC denotes the vertical column. The stratospheric column of *y* can be obtained by subtracting the tropospheric column from the total column, so Eq. (2) can be rewritten as follows:

$$\mathrm{VC}_{\mathrm{CH_4}}^{\mathrm{strat}} = a \cdot \mathrm{VC}_{\mathrm{air}}^{\mathrm{strat}} + b\left(\mathrm{VC}_{y} - \mathrm{VC}_{y}^{\mathrm{trop}}\right) \tag{3}$$

The tropospheric column-averaged mole fraction of the $CH_4$ is then calculated as:

$$X_{\mathrm{CH_4}}^{\mathrm{trop}} = \frac{\mathrm{VC}_{\mathrm{CH_4}} - \mathrm{VC}_{\mathrm{CH_4}}^{\mathrm{strat}}}{\mathrm{VC}_{\mathrm{air}}^{\mathrm{trop}}} \tag{4}$$

In Eq. (3) the tropospheric column of HF is zero. The mole fraction of $N_2O$ is almost constant with respect to altitude in the troposphere. In addition, the seasonal and long-term variation of the $N_2O$ mole fraction is quite small, and therefore highly predictable. So the tropospheric column of $N_2O$ can then be calculated as the product of its mole fraction and the dry air column in the troposphere. The mole fraction of $N_2O$ in the troposphere can be obtained from in situ measurements or a model simulation. The distribution of $N_2O$ is fairly uniform with relatively small variability (3–5 ppb) (Kort et al., 2011). In this paper a simple linear model is applied, an $N_2O$ growth rate of 0.75 ppb yr$^{-1}$ is assumed from a background concentration of 315 ppb at the start of the year 2000 (http://www.esrl.noaa.gov/gmd/hats/combined/N2O.html). The dry air columns in the stratosphere and troposphere are derived as follows: firstly using the surface pressure and the tropopause pressure to calculate these dry air columns,

$$\mathrm{VC}_{\mathrm{air}}^{\mathrm{trop}} = \frac{P_\mathrm{s} - P_\mathrm{t}}{m_{\mathrm{air}}^{\mathrm{dry}} \cdot g(p)} - \mathrm{VC}_{\mathrm{H_2O}} \cdot \frac{m_{\mathrm{H_2O}}}{m_{\mathrm{air}}^{\mathrm{dry}}} \tag{5}$$

$$\mathrm{VC}_{\mathrm{air}}^{\mathrm{strat}} = \frac{P_\mathrm{t}}{m_{\mathrm{air}}^{\mathrm{dry}} \cdot g(p)} \tag{6}$$

where, $P_\mathrm{s}$ and $P_\mathrm{t}$ are surface pressure and tropopause pressure, respectively, $m_{\mathrm{air}}^{\mathrm{dry}}$ and $m_{\mathrm{H_2O}}$ are the molecular mass of dry air and $H_2O$, respectively, and $g(p)$ is the absorber weighted gravitational acceleration. Equation (6) also makes use of the fact that the stratosphere is extremely dry. The surface pressure is obtained from in situ measurements while the tropopause pressure is derived from the NCEP temperature profile. In Eq. (3) instead of using a value derived from ACE-FTS data for constant $a$, we derive it in an alternative fashion. From Eq. (1) when approaching the troposphere the left hand side approaches the $CH_4$ mole fraction at the tropopause, and the right hand side becomes the constant $a$ plus the mole fraction of $y$ at the tropopause multiplied by slope *b*. Since we can assume that the $N_2O$ mole fraction is a constant known quite well and the HF mole fraction is zero throughout the troposphere, we can calculate the constant *a* if we know the $CH_4$ mole fraction at tropopause. This is done iteratively, starting from the constant *a* derived from satellite measurements and then using Eqs. (3) and (4) to calculate the tropospheric column-averaged $CH_4$ mole fraction. Since we need to know the $CH_4$ mole fraction at the tropopause the relative distribution profile of $CH_4$ mole fraction in the troposphere is needed. Here the GFIT a priori profile is assumed. Then this profile of $CH_4$ is scaled so that the tropospheric column-averaged $CH_4$ mole fraction calculated from the scaled a priori profile is equal to that derived using Eqs. (3) and (4). Then the mole fraction value of the scaled a priori $CH_4$ profile at tropopause is used to calculate the new value of the constant *a*. This process is repeated until that the change in the constant *a* is overlooked. Figure 2 gives a comparison between constant *a* derived from the original and scaled GFIT a priori and the satellite data at Spitsbergen.

According to the results of Eqs. (5) and (6), the relative fractions of tropospheric and stratospheric dry air column can be determined. The total dry air column inferred from the $O_2$ column is then separated into tropospheric and stratospheric parts according to these fractions. The dry air columns in the stratosphere and troposphere derived from $O_2$ column are used in Eqs. (3) and (4). Although surface pressure can be measured with better precision than the $O_2$ column, using $O_2$ column takes into account factors that affect $CH_4$, $N_2O$, HF and $O_2$ column retrievals in a common way – pointing/tracking, any light path variations etc. In the calculation above, the water vapor is assumed to be located completely in the troposphere. We also tested the assumption that the retrieved water vapor profile is vertically distributed as described in the a priori (that is, according to the NCEP profile). The two methods produce a difference of less than 0.5 ppb in the derived tropospheric column-averaged mole fraction of $CH_4$, so for simplicity the first method is applied.

### 3.2 Strategy implicitly using tropopause pressure

In the case of the HF, when approaching the tropopause, the HF mole fraction approaches zero and so the constant *a* in Eq. (1) represents $\mathrm{CH_4}$ mole fraction around the tropopause. Washenfelder et al. (2003) consider *a* as the tropospheric column-averaged $\mathrm{CH_4}$ mole fraction, and use $\mathrm{O_2}$ to infer the dry air column. Under these conditions, inserting Eq. (3) into Eq. (4) yields the equation used by them,

$$X_{\mathrm{CH_4}}^{\mathrm{trop}} = a = \frac{0.2095(\mathrm{VC_{CH_4}} - b \cdot \mathrm{VC_{HF}})}{\mathrm{VC}_{O_2}} \qquad (7)$$

This method can be used for $\mathrm{N_2O}$ as well. Since in the troposphere, the $\mathrm{N_2O}$ mole fraction is almost constant and its value can be quite well predicted, we then subtract the tropospheric $\mathrm{N_2O}$ mole fraction from its mole fraction profile in the whole atmosphere. Such a derived “species” will also be present completely in the stratosphere and Eq. (1) also holds as long as the constant *a* is replaced by a value equal to *a* plus the tropospheric $\mathrm{N_2O}$ mole fraction multiplied by the slope *b*, and consider this quantity as the tropospheric column-averaged $\mathrm{CH_4}$ mole fraction. We obtain the following equation,

$$X_{\mathrm{CH_4}}^{\mathrm{trop}} = \frac{\mathrm{VC_{CH_4}} - b\left(\mathrm{VC}_y - X_y^{\mathrm{trop}}\mathrm{VC}_{O_2}/0.2095\right)}{\mathrm{VC}_{O_2}/0.2095} \qquad (8)$$

$X_y^{\mathrm{trop}}$ is replaced by $X_{\mathrm{N_2O}}^{\mathrm{trop}}$ for $\mathrm{N_2O}$ or set to zero for HF. Compared with the strategy in Sect. 3.1, this approach does not use the tropopause pressure to correct for the stratospheric contribution of $\mathrm{CH_4}$ column. The tropopause pressure used here is derived from the NCEP temperature profile and is therefore the thermal tropopause and not necessarily the same as the chemical tropopause. Variation of the location of thermal tropopause from the chemical tropopause will distort the assumption about the vertical distribution of $\mathrm{N_2O}$ and HF. In the implicit strategy, the stratospheric contribution is inferred from variations of the N2O/HF column, which mainly results from variation of the chemical tropopause. So the implicit strategy is free from the influence of inaccuracy in tropopause pressure.

### 3.3 Accounting for the averaging kernel effect

Due to the effect of the averaging kernel the straightforward equations above (Eqs. 4 and 8) need to be modified. The total column retrieved by GFIT is a weighted summation of partial columns at different altitudes. The weights are represented by the averaging kernel and a pressure weighting function that usually differs from one. The partial column reflected in the retrieved total column will be very different from its original value. Figure 3 presents the averaging kernels of HF, $N_2O$ and $CH_4$ for Bialystok from all spectra during 2010. The averaging kernel mainly depends on the solar zenith angle. In the case of $N_2O$, the averaging kernel has a large weight in stratosphere and small weight in troposphere, so variations in the stratospheric column of $N_2O$ will be amplified in the retrieved total column compared to the true atmospheric variability, and tropospheric variations will be dampened. For $CH_4$, the averaging kernel is close to unity at all altitudes, so the effect of the averaging kernel is small. From Rodgers (2000) and Wunch et al. (2010) the mole fraction profile retrieved by a profile-scaling retrieval, such as that performed by GFIT, is:

$$x_\mathrm{r} = x_\mathrm{a} + A\,(x_\mathrm{t} - x_\mathrm{a}) \tag{9}$$

where, the $x_\mathrm{r}$, $x_\mathrm{t}$ and $x_\mathrm{a}$ are the retrieved, true and a priori mole fraction profile, respectively. $A$ is the averaging kernel. Integrating Eq. (10) and rearranging yields:

$$\int_0^{P_\mathrm{s}} x_\mathrm{r} \frac{\mathrm{d}p}{mg} = \int_0^{P_\mathrm{s}} (I - A)x_a \frac{\mathrm{d}p}{mg} + \int_0^{P_\mathrm{s}} A\left(x_\mathrm{t}^\mathrm{strat} + x_\mathrm{t}^\mathrm{trop}\right)\frac{\mathrm{d}p}{mg} \tag{10}$$

where, $m$ is the molecular mass of moist air (i.e. $m = \left(1 - x_{\mathrm{H_2O}}\right) m_\mathrm{dry}^\mathrm{air} + x_{\mathrm{H_2O}} \cdot m_{\mathrm{H_2O}}$), $g$ is the gravitational acceleration and I is the identity matrix. In Eq. (10), the true mole fraction profile is separated into stratospheric and tropospheric components. Because GFIT performs a profile scaling retrieval and produces the column averaging kernel vector (Connor, 2009) instead of a full averaging kernel matrix, when using a column averaging kernel Eq. (10) can be rewritten as:

$$\int_{0}^{P_\mathrm{s}} x_\mathrm{r}\frac{\mathrm{d}p}{mg} = \int_{0}^{P_\mathrm{s}} (1-a(p))x_a\frac{\mathrm{d}p}{mg} + \int_{P_\mathrm{t}}^{P_\mathrm{s}} a(p)x_\mathrm{t}\frac{\mathrm{d}p}{mg} + \int_{0}^{P_\mathrm{t}} a(p)x_\mathrm{t}\frac{\mathrm{d}p}{mg} \tag{11}$$

where $a(p)$ is the column averaging kernel vector, which is a function of pressure (altitude). It can be seen from the equation above that there are three terms contributing to the retrieved total column: the a priori profile, and the tropospheric and stratospheric columns. We then define the following relationships:

$$\alpha = \frac{\int_{P_\mathrm{t}}^{P_\mathrm{s}} x_\mathrm{t}\frac{\mathrm{d}p}{mg}}{\int_{P_\mathrm{t}}^{P_\mathrm{s}} a(p)x_\mathrm{t}\frac{\mathrm{d}p}{mg}} \tag{12}$$

$$\beta = \frac{\int_{0}^{P_\mathrm{t}} x_\mathrm{t}\frac{\mathrm{d}p}{mg}}{\int_{0}^{P_\mathrm{t}} a(p)x_t\frac{\mathrm{d}p}{mg}} \tag{13}$$

$$\gamma = \int_{0}^{P_\mathrm{s}} (1-a(p))x_a\frac{\mathrm{d}p}{mg} \tag{14}$$

$\alpha$ is the ratio of the true tropospheric column to that reflected in the retrieved column, $\beta$ has a same meaning for the stratosphere, and $\gamma$ is the a priori part of the retrieved column. To account for the effect of the averaging kernel, Eqs. (3) and (4) are be modified to give:

$$\mathrm{VC}_{\mathrm{CH_4}}^{\mathrm{strat}} = a \cdot \mathrm{VC}_{\mathrm{air}}^{\mathrm{strat}} + b \cdot \beta_y \left(\mathrm{VC}_y - \mathrm{VC}_y^{\mathrm{trop}} \cdot \alpha_y^{-1} - \gamma_y\right) \tag{15}$$

$$X_{\mathrm{CH_4}}^{\mathrm{trop}} = \frac{\alpha_{\mathrm{CH_4}} \left(\mathrm{VC}_{\mathrm{CH_4}} - \mathrm{VC}_{\mathrm{CH_4}}^{\mathrm{strat}} \cdot \beta_{\mathrm{CH_4}}^{-1} - \gamma_{\mathrm{CH_4}}\right)}{\mathrm{VC}_{\mathrm{air}}^{\mathrm{trop}}} \tag{16}$$

In Eq. (15), multiplying $\mathrm{VC}_y^{\mathrm{trop}}$ by the inverse of $\alpha_y$ takes retrieval sensitivity of $y$ in the tropospheric part into account. Subtracting $\mathrm{VC}_y^{\mathrm{trop}} \cdot \alpha_y^{-1}$ and $\gamma_y$ from the retrieved total column $\mathrm{VC}_y$ yields the stratospheric column of $y$ reflected in its retrieved total column. Then multiplying by $\beta_y$ removes retrieval sensitivity in the stratospheric column of $y$. In Eq. (16), multiplying $\mathrm{VC}_{\mathrm{CH_4}}^{\mathrm{strat}}$ by the inverse of $\beta_{\mathrm{CH_4}}$ takes retrieval sensitivity of $\mathrm{CH_4}$ to the stratospheric part into account. Subsequently subtracting $\mathrm{VC}_{\mathrm{CH_4}}^{\mathrm{strat}} \cdot \beta_{\mathrm{CH_4}}^{-1}$ and $\gamma_{\mathrm{CH_4}}$ from the retrieved total column gives the tropospheric column reflected in the retrieved column, and multiplying it with $\alpha_{\mathrm{CH_4}}$ removes retrieval sensitivity in the tropospheric column of $\mathrm{CH_4}$. These coefficients $\alpha$ and $\beta$ depend on the shape of true mole fraction profile, which is unknown. So the a priori profile is used to calculate the approximate value of these coefficients. The effectiveness of removing or taking retrieval sensitivity into account in the manipulation above will depend on the difference between the shapes of the true and a priori mole fraction profiles. This could introduce additional error.

The error introduced by using Eqs. (3) and (4) is the smoothing error in the total column, and that using the Eqs. (15) and (16) is the error of the coefficients $\alpha$ and $\beta$. It can be explained as follows, in Eq. (3) the total column of $y$ can be expressed as:

$$\mathrm{VC}_y = \int_0^{P_\mathrm{s}} x_\mathrm{t}^y \frac{\mathrm{d}p}{mg} + \int_0^{P_\mathrm{s}} \left(1 - a_y(p)\right) \left(x_\mathrm{a}^y - x_\mathrm{t}^y\right) \frac{\mathrm{d}p}{mg} \tag{17}$$

The second term on the right of Eq. (17) is the smoothing error. Inserting Eq. (17) into Eq. (3) yields:

$$\mathrm{VC}_{\mathrm{CH_4}}^{\mathrm{strat}} = a \cdot \mathrm{VC}_{\mathrm{air}}^{\mathrm{strat}} + b \left( \int_0^{P_\mathrm{s}} x_\mathrm{t}^y \frac{\mathrm{d}p}{mg} + \int_0^{P_\mathrm{s}} (1 - a_y(p)) \left( x_\mathrm{a}^y - x_\mathrm{t}^y \right) \frac{\mathrm{d}p}{mg} - \mathrm{VC}_y^{\mathrm{trop}} \right) \tag{18}$$

Without accounting for the error in the tropospheric column of $y$, the term in brackets on the right of Eq. (18) is just the true stratospheric column of $y$ plus the smoothing error. For Eq. (15), where the equation accounts for the averaging kernel effect, when the a priori profile is used to calculate the coefficients $\alpha$ and $\beta$ it can rewritten as:

$$\mathrm{VC}_{\mathrm{CH_4}}^{\mathrm{strat}} = a \cdot \mathrm{VC}_{\mathrm{air}}^{\mathrm{strat}} + b \cdot \frac{\int_0^{P_\mathrm{t}} x_\mathrm{a}^y \frac{\mathrm{d}p}{mg}}{\int_0^{P_\mathrm{t}} a_y(p) x_a^y \frac{\mathrm{d}p}{mg}} \left( \mathrm{VC}_y - \mathrm{VC}_y^{\mathrm{trop}} \cdot \frac{\int_{P_\mathrm{t}}^{P_\mathrm{s}} a_y(p) x_a^y \frac{\mathrm{d}p}{mg}}{\int_{P_\mathrm{t}}^{P_\mathrm{s}} x_\mathrm{a}^y \frac{\mathrm{d}p}{mg}} - \gamma_y \right) \tag{19}$$

Inserting Eq. (17) into Eq. (19) and overlooking the error in the tropospheric column of $y$ yields:

$$\begin{aligned} \mathrm{VC}_{\mathrm{CH_4}}^{\mathrm{strat}} = a \cdot \mathrm{VC}_{\mathrm{air}}^{\mathrm{strat}} + b \cdot & \left( \frac{\int_0^{P_\mathrm{t}} x_\mathrm{t}^y \frac{\mathrm{d}p}{mg}}{\int_0^{P_\mathrm{t}} a_y(p) x_\mathrm{t}^y \frac{\mathrm{d}p}{mg}} + e_1 \right) \\ & \left[ \int_0^{P_\mathrm{s}} a_y(p) x_\mathrm{t}^y \frac{\mathrm{d}p}{mg} - \int_{P_\mathrm{t}}^{P_\mathrm{s}} x_\mathrm{t}^y \frac{\mathrm{d}p}{mg} \cdot \left( \frac{\int_{P_\mathrm{t}}^{P_\mathrm{s}} a_y(p) x_t^y \frac{\mathrm{d}p}{mg}}{\int_{P_\mathrm{t}}^{P_\mathrm{s}} x_\mathrm{t}^y \frac{\mathrm{d}p}{mg}} + e_2 \right) \right] \end{aligned} \tag{20}$$

Where $e_1$ and $e_2$ are the errors related to the coefficients $\alpha$ and $\beta$,

$$e_1 = \frac{\int_0^{P_\mathrm{t}} x_\mathrm{a}^y \frac{\mathrm{d}p}{mg}}{\int_0^{P_\mathrm{t}} a_y(p) x_\mathrm{a}^y \frac{\mathrm{d}p}{mg}} - \frac{\int_0^{P_\mathrm{t}} x_\mathrm{t}^y \frac{\mathrm{d}p}{mg}}{\int_0^{P_\mathrm{t}} a_y(p) x_\mathrm{t}^y \frac{\mathrm{d}p}{mg}} \tag{21}$$

$$e_2 = \frac{\int_{P_t}^{P_s} a_y(p) x_a^y \frac{dp}{mg}}{\int_{P_t}^{P_s} x_a^y \frac{dp}{mg}} - \frac{\int_{P_t}^{P_s} a_y(p) x_t^y \frac{dp}{mg}}{\int_{P_t}^{P_s} x_t^y \frac{dp}{mg}} \tag{22}$$

Rearranging the terms in Eq. (20) produces,

$$\mathrm{VC}_{\mathrm{CH_4}}^{\mathrm{strat}} = a \cdot \mathrm{VC}_{\mathrm{air}}^{\mathrm{strat}} + b \cdot \left( \int_0^{P_t} x_t^y \frac{dp}{mg} + \int_0^{P_t} a_y(p) x_t^y \frac{dp}{mg} \cdot e_1 - \int_{P_t}^{P_s} x_t^y \frac{dp}{mg} \cdot \frac{\int_0^{P_t} x_a^y \frac{dp}{mg}}{\int_0^{P_t} a_y(p) x_a^y \frac{dp}{mg}} \cdot e_2 \right) \tag{23}$$

Similar to Eq. (18), the term in brackets is the true stratospheric column of $y$ plus an error term that is different from the smoothing error. The smoothing error depends on the difference between the shapes of true mole fraction profile and the a priori, and also the overall inhomogeneity of the averaging kernel in the whole atmosphere. The smoothing error increases with an increase in the inhomogeneity of the averaging kernel. However the error term in Eq. (23) depends on $e_1$ and $e_2$, which depend on the inhomogeneity of the averaging kernel and the difference between the shapes of the true and a priori mole fraction profiles in only the stratosphere and troposphere, respectively. It can be seen more clearly using another form:

$$e_2 = \frac{\int_{P_t}^{P_s} \int_{P_t}^{P_s} \left[a_y(p_1) - a_y(p_2)\right] x_a^y(p_1) x_t^y(p_2) \frac{dp_1}{mg} \frac{dp_2}{mg}}{\int_{P_t}^{P_s} \int_{P_t}^{P_s} x_a^y(p_1) x_t^y(p_2) \frac{dp_1}{mg} \frac{dp_2}{mg}} \tag{24}$$

In Eq. (24), the term $\left[a_y(p_1) - a_y(p_2)\right]$ is an anti-symmetric function about line $p_1 = p_2$ on plane $(p_1, p_2)$ and term $x_a^y(p_1) x_t^y(p_2)$ is a symmetric function about this line provided the true mole fraction and the a priori profiles have the same shape in the troposphere. So, $e_2$ depends on the amplitude of the first term, which is the inhomogeneity of the averaging kernel in the troposphere, and the symmetry of the second term. Similar arguments can be applied to $e_1$. The difference between the stratospheric and tropospheric parts of the averaging kernel does not contribute to the error term in Eq. (23). In this sense the effect of the averaging kernel is removed since in our calculation the atmosphere is viewed as consisting of only two layers, the stratosphere and troposphere. In addition the equation accounting for the averaging kernel effect does not apply to HF becuase it is solely present in the stratosphere.

Similarly for the strategy implicitly using tropopause pressure, after taking the averaging kernel effect into account we get the following equations.

$$X_{\mathrm{CH_4}}^{\mathrm{trop}} = \frac{\mathrm{VC_{CH_4}} - \gamma_{\mathrm{CH_4}} - b\mu_y \left(\mathrm{VC}_y - \gamma_y - \varphi_y \cdot X_y^{\mathrm{trop}} \cdot \mathrm{VC_{O_2}}/0.2095\right)}{\varphi_{\mathrm{CH_4}} \cdot \mathrm{VC_{O_2}}/0.2095} \tag{25}$$

$$\varphi = \int_0^{P_\mathrm{s}} a \frac{\mathrm{d}p}{mg} \Big/ \int_0^{P_\mathrm{s}} \frac{\mathrm{d}p}{mg} \tag{26}$$

$$\mu = \int_0^{P_\mathrm{t}} a_{\mathrm{CH_4}} \left(x_\mathrm{t} - x_\mathrm{t}^{\mathrm{trop}}\right) \frac{\mathrm{d}p}{mg} \Big/ \int_0^{P_\mathrm{t}} a \left(x_\mathrm{t} - x_\mathrm{t}^{\mathrm{trop}}\right) \frac{\mathrm{d}p}{mg} \tag{27}$$

For calculation of the coefficients $\varphi$ and $\mu$, the true mole fraction profiles of $N_2O$ and HF are replaced by the GFIT a priori profile, and in the case of $N_2O$, the a priori profile is scaled to fit the tropospheric $N_2O$ mole fraction we assumed before. $x_y^{\mathrm{trop}}$ is replaced by $X_{\mathrm{N_2O}}^{\mathrm{trop}}$ for $N_2O$ or set to zero for HF.

To compare the derived tropospheric column-averaged $CH_4$ mole fraction with in situ measurements, the measured $CH_4$ profiles need to be integrated. At the same time, the averaging kernel of the FTS measurements needs to be taken into account. For our purpose only the tropospheric profile is important, and here we are only considering the case of the strategy implicitly using tropopause pressure. After replacing the total column in the right side of Eq. (25) by the right side of Eq. (10), assuming the coefficient defined by Eq. (27) accurately replaces the averaging kernels of $N_2O$ or HF with ones of $CH_4$, and applying Eq. (1) in stratospheric part, it can then be seen that the effect of averaging kernel can be represented as:

$$X^{\mathrm{trop}}_{\mathrm{CH_4}} = \frac{\int_{P_\mathrm{t}}^{P_\mathrm{s}} a_{\mathrm{CH_4}} x_\mathrm{t} \frac{\mathrm{d}p}{mg}}{\int_{P_\mathrm{t}}^{P_\mathrm{s}} a_{\mathrm{CH_4}} \frac{\mathrm{d}p}{mg}} \tag{28}$$

to integrate the aircraft data, with $x_\mathrm{t}$ simply replaced by the in situ profile.

### 3.4 Taking calibration factors into account

The derivations above are based on the total columns of $\mathrm{CH_4}$, $\mathrm{N_2O}$ and HF, but the total columns directly retrieved from the spectra include errors arising from spectroscopy imperfections and instrumental effects. The final TCCON products are the dry air column averaged mole fraction $X_{\mathrm{CH_4}}$, $X_{\mathrm{N2O}}$ and $X_{\mathrm{HF}}$, which have been corrected by airmass independent and airmass dependent calibration factors to account for such errors. These corrections should be taken into account for this work. For the strategy explicitly using tropopause pressure, after combining Eqs. (15) and (16) the final equation becomes,

$$X^{\mathrm{trop}}_{\mathrm{CH_4}} = \frac{\alpha_{\mathrm{CH_4}}}{f}\left\{X_{\mathrm{CH_4}} - \left[a(1-f) + b\cdot\beta_y\left(X_y - X_y^{\mathrm{trop}}\cdot f\cdot\alpha_y^{-1} - \frac{\gamma_y}{\mathrm{VC_{air}}}\right)\right]\beta_{\mathrm{CH_4}}^{-1} - \frac{\gamma_{\mathrm{CH_4}}}{\mathrm{VC_{air}}}\right\}, \tag{29}$$

where, $f$ is the fraction of the tropospheric dry air column in the total dry air column, and $\mathrm{VC_{air}}$ is the summation of the left hand sides of Eqs. (5) and (6). For the strategy implicitly using tropopause pressure, the Eq. (26) can be written as:

$$X^{\mathrm{trop}}_{\mathrm{CH_4}} = \frac{1}{\varphi_{\mathrm{CH_4}}}\left[X_{\mathrm{CH_4}} - \frac{\gamma_{\mathrm{CH_4}}}{\mathrm{VC_{air}}} - b\cdot\mu_y\left(X_y - \frac{\gamma_y}{\mathrm{VC_{air}}} - \varphi_y\cdot X_y^{\mathrm{trop}}\right)\right] \tag{30}$$

The airmass independent calibration factors are taken as those used throughout TCCON (Wunch et al., 2010). These factors have been re-evaluated by Geibel (2012) based on European sites, but this reevaluation is not taken into account because it has not been applied to the current TCCON release.

## 4 Results

To test the method described in Sect. 3, data from four TCCON sites at Spitsbergen, Orléans, Bialystok and Darwin are used. Figure 4 presents the comparison for the two strategies described in Sect. 3 at Spitsbergen in the case of $N_2O$, since only at this site do the two methods produce a significant difference. The method explicitly using tropopause pressure results in a larger value in comparison with in situ data in winter time. This might arise from an error in the tropopause pressure derived from the NCEP temperature profile. During wintertime the tropopause is lower and this method is more sensitive to such an error. The seasonal cycle amplitude in tropospheric column-averaged $CH_4$ mole fraction resulting from the method implicitly using tropopause pressure is weaker than that observed in collocated in situ data. It is not clear how the in situ data differ from tropospheric column-averaged value at this site. In the case of HF, the method explicitly using tropopause pressure also produce higher value, but the difference is only around 10 ppb around. In the iteration process of the method explicitly using tropopause pressure, the vertical distribution of $CH_4$ in the troposphere should be known to derive $CH_4$ mole fraction at tropopause from the tropospheric column-averaged concentration. The GFIT a priori distribution is assumed here. So, for all the following results, the strategy implicitly using tropopause pressure is applied.

### 4.1 Comparison between the $N_2O$ and HF methods and in situ data

Figures 5–8 show the results for Spitsbergen, Orléans, Bialystok and Darwin. We compare to in situ data from NOAA at Spitsbergen, and the low aircraft data at Orléans and Bialystok. These profiles have been extended into whole troposphere as described in Sect. 2.2, and then integrated to produce a tropospheric column-averaged $CH_4$ mole fraction. At all sites with in situ data available for comparison the results using $N_2O$ are closer to the in situ measurements than when using HF. The difference between the results using $N_2O$ and HF has both seasonal and site dependence. At Spitsbergen the

Title Page
Abstract | Introduction
Conclusions | References
Tables | Figures
◀| |▶
◀ ▶
Back | Close
Full Screen / Esc
Printer-friendly Version
Interactive Discussion

results using $N_2O$ are about 30 ppb higher than that using HF, about 20 ppb at Bialystok and Orléans, and about −10 ppb around at Darwin. Such difference might result from the uncertainty in the HF column. The HF column used here is not calibrated through in situ profile measurements since HF is located completely in the stratosphere and there are no such measurements currently available. Inaccuracy in the spectroscopy of HF will force the retrieved HF column away from the truth. Such an effect also depends on the HF total column. A stronger signal is more sensitive to a spectroscopy parameter error. This might partly explain the site dependence of the difference between the results using $N_2O$ and HF since every site has its own characteristic tropopause pressure and HF column.

Another difference is that the results using HF have more scatter at Darwin than at the other three sites, however, results using $N_2O$ have similar scatter for all four sites. This difference also arises from HF column error. In the NIR the HF column is retrieved from a weak spectral absorption line that is located at the shoulder of a water line. Therefore, the retrieval of HF suffers from water vapor interference. Such influence depends on both the water amount and its vertical distribution, and results in more scatter. In the tropics the higher amount of water vapor in atmosphere will influence HF column significantly. Another factor is that HF is completely located in the stratosphere, and since generally the tropopause height increase from high to low latitude, the column amount of HF decreases. Retrieval of HF has better precision and worse accuracy for the case of larger HF column due to more significant signal and larger effect from spectroscopy error respectively, and vice versa. The performance of the HF method should be more stable but have a larger offset for high-latitude sites like Spitsbergen owing to the dry conditions and more significant signals, and be less stable and have a smaller offset for tropical sites like Darwin because of the moisture conditions and relatively weaker signals.

The main problem in the $N_2O$ approach is that we assume a constant $N_2O$ mole fraction throughout the troposphere. This is a reasonable approximation because of its long life time in the atmosphere (114 yr). However, in presence of local sources, like biomass burning and industrial sources, depending on the strength of the sources such an assumption might not be valid. As the same tropospheric $N_2O$ mole fraction is used for all sites, the difference between different regions is also neglected. This can also cause problem for site where there are strong local $N_2O$ sources. Sensitivity test reveals that a 2 ppb perturbation in assumed tropospheric $N_2O$ mole fraction (an estimation of its seasonal cycle amplitude) results in perturbation in the derived tropospheric column-averaged $CH_4$ mole fraction of $4.0 \sim 4.4$ ppb at Darwin, $4.2 \sim 5.6$ ppb at Orléans and $4.5 \sim 5.5$ ppb at Spitsbergen.

### 4.2 Comparison with aircraft profile data

In situ profiles from the aircraft campaigns HIPPO and IMECC are used to compare the derived tropospheric column-averaged $CH_4$ mole fraction and assess the inter-site consistency of the methods. Figure 9 shows the results. The aircraft data at Bialystok and Orléans are from the IMECC campaign, and at Darwin from the HIPPO-4 campaign. According to definition, the tropospheric column-averaged $CH_4$ mole fraction is the mean abundance between the surface and the chemical tropopause. The aircraft profiles do not extend high enough to identify the chemical tropopause, so instead the thermal tropopause is used. The GFIT a priori profile is used for altitudes between the highest sample and the tropopause altitude. The a priori profile has been scaled to match the aircraft profile in the sampled tropospheric part. The mole fraction at the lowest sample point is extended to the surface to complete the profile below the lowest measured point during the aircraft flight.

The constructed profiles are then integrated using Eq. (28). Results from FTIR during the aircraft measurement period are averaged to give a final value. The uncertainty of FTIR data is estimated as the standard deviation of these results. The uncertainty of the tropospheric $CH_4$ integrated from the aircraft profile is calculated as the mean of the uncertainties at all sample points along the altitude axis, weighted with the partial air column represented by each point. Comparison between GFIT a priori and in situ measurements reveals that the standard deviation of ratios of a priori to measurement is 1.8 %. For the altitude range where the scaled GFIT a priori is used an uncertainty of 1.8 % is assumed. This represents the largest contribution to the total uncertainty. The uncertainties for the points above the aircraft ceiling are estimated from instrumental performance and variation of $CH_4$ mole fraction along the aircraft path. In general the results using $N_2O$ more closely fall on the fitted line. The distances between scatter points and fitted line are 3.5, 4.6, 2.1, 0.8, 0.2, 5.7 ppb for results derived using the $N_2O$ and 7.6, 9.0, 6.9, 0.4, 7.1, 17.2 ppb for the HF method.

## 5 Uncertainty analysis

The Gaussian error propagation equation is used to estimate the uncertainty in calculating the tropospheric column-averaged mole fraction of $CH_4$ using Eq. (30). The variation of tropospheric mole fraction of $N_2O$ during one day is small and might cause bias that varies on seasonal time scale. We concentrate on the estimation of precision here. So the errors in the assumed tropospheric mole fraction of $N_2O$ were not taken into account. Besides, the errors in the coefficients accounting for the averaging kernel effect are overlooked as well since they are unknown. The errors of the slope parameters (b) are estimated as 0.011 ($N_2O$) and 1.9 (HF).

The errors of the $XCH_4$, $XN_2O$ and XHF are taken as the uncertainties estimated in GFIT. As an alternative approach of estimating the uncertainty, we calculate the standard deviation of the derived tropospheric column-averaged $CH_4$ mole fractions during a day. To ensure the calculated standard deviation is meaningful and that days with fine weather condition are considered, only those days with more than 50 spectra available at Spitsbergen and 100 spectra available at other sites are used. Figure 10 presents the estimated relative uncertainty for all sites using Gaussian error propagation equation method and Fig. 11 presents results using the standard deviation method. The two methods produce results with similar behavior. The mean relative standard deviation of tropospheric column-averaged $CH_4$ mole fraction using $N_2O$ is 0.15 (Darwin), 0.30 (Spitsbergen), 0.28 (Orléans) and 0.14 (Bialystok) percent, and 0.93, 0.45, 0.50, 0.20 % respectively in the case of HF. So the method using HF produces larger uncertainties, especially at Darwin. Also the uncertainty of the method using HF has a stronger $H_2O$ dependence. This is because the retrieval of HF column suffers strong interference from $H_2O$, and so does the derived tropospheric column-averaged $CH_4$ mole fraction.

## 6 Conclusions

In this paper, we propose using $N_2O$ to correct for the stratospheric contribution to the total column of $CH_4$ in order to derive a tropospheric column-averaged $CH_4$ mole fraction. This method is applied to four TCCON sites data. At Spitsbergen and Orléans, the tropospheric $CH_4$ derived using $N_2O$ and HF are compared with surface flask measurements and low aircraft profiles data, respectively. At both sites, the results using $N_2O$ agree better with in situ measurements than the HF derived results. Uncertainty analysis reveals that $N_2O$ method results in smaller uncertainty than HF at all sites. The mean relative standard deviations are 0.23 % and 0.52 % for the methods using $N_2O$ and HF, respectively. Especially, at Darwin the HF method produces much larger uncertainty (0.93 % compared with 0.15 % of $N_2O$ method), which clearly indicates a dependence on $H_2O$ that is absent for the $N_2O$ method. This $N_2O$ method has also been compared with aircraft profiles at three sites, and the result reveals that $N_2O$ method has better inter-site consistency. The sensitivity of the derived tropospheric $CH_4$ to the assumed tropospheric $N_2O$ mole fraction is 4 ~ 5 ppb per 2 ppb. Further work can be done to represent $N_2O$ mole fraction in troposphere more realistically.

*Acknowledgements.* This work was funded by the EU-project InGOS. Furthermore the authors acknowledge the EU-projects ICOS-INWIRE for support of the measurements, the EU-project IMECC for the aircraft data at Orleans and Bialystok, additional funding for IMECC aircraft data by the Max Plank Society, and the sponsors of the HIPPO project: the National Science Foundation, the National Oceanic and Atmospheric Administration and G-V “HIAPER”: National

Center for atmospheric Research and Steven C. Wofsy for providing aircraft data at Darwin. We thank NOAA, Earth System Research Laboratory, Global Monitoring Division for providing surface CH4 flask data.

## References

Avallone, L. M. and Prather, M. J.: Tracer-tracer correlations: three-dimensional model simulations and comparisons to observations, J. Geophys. Res., 102, 19233–19246, 1997.

Bernath, P. F., McElroy, C. T., Abrams, M. C., Boone, C. D., Butler, M., Camy-Peyret, C., Carleer, M., Clerbaux, C., Coheur, P.-F., Colin, R., DeCola, P., DeMazière, M., Drunnond, J. R., Dufour, D., Evans, W. F. J., Fast, H., Fussen, D., Gilber, K., Jennings, D. E., Llewellyn, E. J., Lowe, R. P., Mahieu, E., McConnell, J. C., McHugh, M., McLeod, S. D., Michaud, R., Midwinter, C., Nassar, R., Nichitiu, F., Nowlan, C., Rinsland, C. P., Rochon, Y. ., Rolands, N., Sememiuk, K., Simom, P., Skelton, R., Sloan, J. J., Soucy, M.-A., Strong, K., Tremblay, P., Turnbull, D., Walker, K. A., Walkty, I., Wardle, D. A., Wehrle, V., Zander, R., and Zou, J.: Atmospheric Chemistry Experiment (ACE): mission overview, Geophys. Res. Lett., 32, L15S01, doi:10.1029/2005GL022386, 2005.

Bousquet, P., Ringeval, B., Pison, I., Dlugokencky, E. J., Brunke, E.-G., Carouge, C., Chevallier, F., Fortems-Cheiney, A., Frankenberg, C., Hauglustaine, D. A., Krummel, P. B., Langenfelds, R. L., Ramonet, M., Schmidt, M., Steele, L. P., Szopa, S., Yver, C., Viovy, N., and Ciais, P.: Source attribution of the changes in atmospheric methane for 2006–2008, Atmos. Chem. Phys., 11, 3689–3700, doi:10.5194/acp-11-3689-2011, 2011.

Connor, B.: Column averaging kernel definition, for TCCON community available at: https://tccon-wiki.caltech.edu/Software/GGG/Averaging_Kernels (last access: 12 February 2013), 2009.

Deutscher, N. M., Griffith, D. W. T., Bryant, G. W., Wennberg, P. O., Toon, G. C., Washenfelder, R. A., Keppel-Aleks, G., Wunch, D., Yavin, Y., Allen, N. T., Blavier, J.-F., Jiménez, R., Daube, B. C., Bright, A. V., Matross, D. M., Wofsy, S. C., and Park, S.: Total column $CO_2$ measurements at Darwin, Australia – site description and calibration against in situ aircraft profiles, Atmos. Meas. Tech., 3, 947–958, doi:10.5194/amt-3-947-2010, 2010.

Dlugokencky, E. J., Bruhwiler, L., White, J. W. C., Emmons, L. K., Novelli, P. C., Montzka, S. A., Masarie, K. A., Lang, P. M., Crotwell, A. M., Miller, J. B., and Gatti, L. V.: Observational constraints on recent increases in the atmospheric $CH_4$ burden, Geophys. Res. Lett., 36, L18803, doi:10.1029/2009GL039780, 2009.

Dlugokencky, E. J., Lang, P. M., Crotwell, A. M., Masarie, K. A., and Crotwell, M. J.: Atmospheric Methane Dry Air Mole Fractions from the NOAA ESRL Carbon Cycle Cooperative Global Air Sampling Network, 1983–2012, Version: 2013-08-28, available at: ftp://aftp.cmdl.noaa.gov/data/trace_gases/ch4/flask/surface/ (last access: 12 February 2013), 2013.

Geibel, M. C., Messerschmidt, J., Gerbig, C., Blumenstock, T., Chen, H., Hase, F., Kolle, O., Lavrič, J. V., Notholt, J., Palm, M., Rettinger, M., Schmidt, M., Sussmann, R., Warneke, T., and Feist, D. G.: Calibration of column-averaged $CH_4$ over European TCCON FTS sites with airborne in-situ measurements, Atmos. Chem. Phys., 12, 8763–8775, doi:10.5194/acp-12-8763-2012, 2012.

Herman, R. L., Scott, D. C., Webster, C. R., May, R. D., Moyer, E. J., Salawitch, R. J., Yung, Y. L., Toon, G. C., Sen, B., Margitan, J. J., Rosenlof, K. H., Michelson, H. A., and Elkins, J. W.: Tropical entrainment timescales inferred from stratospheric $N_2O$ and $CH_4$ observations, Geophys. Res. Lett., 25, 2781–2784, 1998.

Kort, E. A., Patra, P. K., Ishijima, K., Daube, B. C., Jiménez, R., Elkins, J., Hurst, D., Moore, F. L., Sweeney, C., and Wofsy, S. C.: Tropospheric distribution and variability of $N_2O$: evidence for strong tropical emissions, Geophys. Res. Lett., 38, L15806, doi:10.1029/2011GL047612, 2011.

Kalnay, K., Kanamitsu, M., Kistler, R., Collins, W., Deaven, D., Candin, L., Iredell, M., Saha, S., White, G., Woollen, J., Zhu, Y., Leetmaa, A., Reynolds, R., Chelliah, M., Ebisuzaki, W., Higgins, W., Janowiak, J., Mo, K. C., Ropelewski, C., Wang, J., Jenne, R., and Joseph, D.: The NCEP/NCAR 40-year reanalysis project, B. Am. Meteorol. Soc., 77, 437–470, 1996.

Messerschmidt, J., Macatangay, R., Notholt, J., Petri, C., Warneke, T., and Weinzierl, C.: Side by side measurements of $CO_2$ by ground-based Fourier transform spectrometry (FTS), Tellus B, 62, 749–758, 2010.

Messerschmidt, J., Chen, H., Deutscher, N. M., Gerbig, C., Grupe, P., Katrynski, K., Koch, F.-T., Lavrič, J. V., Notholt, J., Rödenbeck, C., Ruhe, W., Warneke, T., and Weinzierl, C.: Automated ground-based remote sensing measurements of greenhouse gases at the Białystok site in comparison with collocated in situ measurements and model data, Atmos. Chem. Phys., 12, 6741–6755, doi:10.5194/acp-12-6741-2012, 2012.

Montzka, S. A., Dlugokencky, E. J., and Butler, J. H.: Non-$CO_2$ greenhouse gases and climate change, Nature, 43, 476, doi:10.1038/nature10322, 2011.

Michelson, H. A., Manney, G. L., Gunson, M. R., Rinsland, C. P., and Zander, R.: Correlations of stratospheric abundances of $CH_4$ and $N_2O$ derived from ATMOS measurements, Geophys. Res. Lett., 25, 2777–2780, 1998.

Pałm, M., Melsheimer, C., Noël, S., Heise, S., Notholt, J., Burrows, J., and Schrems, O.: Integrated water vapor above Ny Ålesund, Spitsbergen: a multi-sensor intercomparison, Atmos. Chem. Phys., 10, 1215–1226, doi:10.5194/acp-10-1215-2010, 2010.

Pison, I., Ringeval, B., Bousquet, P., Prigent, C., and Papa, F.: Stable atmospheric methane in the 2000s: key-role of emissions from natural wetlands, Atmos. Chem. Phys., 13, 11609–11623, doi:10.5194/acp-13-11609-2013, 2013.

Plumb, R. A. and Ko, M. K. W.: Interrelationships between mixing ratios of long lived stratospheric constituents, J. Geophys. Res.-Atmos., 97, 10145–10156, 1992.

Rigby, M., Prinn, R. G., Fraser, P. J., Simmonds, P. G., Langenfelds, R. L., Huang, J., Cunnold, D. M., Steele, L. P., Krummel, P. B., Weiss, R. F., O'Doherty, S., Salameh, P. K., Wang, H. J., Harth, C. M., Muehle, J., and Porter, L. W.: Renewed growth of atmospheric methane, Geophys. Res. Lett., 35, L22805, doi:10.1029/2008GL036037, 2008.

Rodgers, C. D.: Inverse Methods for Atmospheric Sounding: Theory and Praxis, ISBN 981-02-2740-X, World Scientific Publishing Co., Singapore, 2000.

Sepúlveda, E., Schneider, M., Hase, F., García, O. E., Gomez-Pelaez, A., Dohe, S., Blumenstock, T., and Guerra, J. C.: Long-term validation of tropospheric column-averaged $CH_4$ mole fractions obtained by mid-infrared ground-based FTIR spectrometry, Atmos. Meas. Tech., 5, 1425–1441, doi:10.5194/amt-5-1425-2012, 2012.

Sussmann, R., Ostler, A., Forster, F., Rettinger, M., Deutscher, N. M., Griffith, D. W. T., Hannigan, J. W., Jones, N., and Patra, P. K.: First intercalibration of column-averaged methane from the Total Carbon Column Observing Network and the Network for the Detection of Atmospheric Composition Change, Atmos. Meas. Tech., 6, 397–418, doi:10.5194/amt-6-397-2013, 2013.

Warneke, T., Meirink, J. F., Bergamaschi, P., Grooß, J.-U., Notholt, J., Toon, G. C., Velazco, V., Goede, A. P. H., and Schrems, O.: Seasonal and latitudinal variation of atmospheric methane: a ground-based and ship-borne solar IR spectroscopic study, Geophys. Res. Lett., 33, L14812, doi:10.1029/2006GL025874, 2006.

Washenfelder, R. A., Wennberg, P. O., and Toon, G. C.: Tropospheric methane retrieved from ground-based near-IR solar absorption spectra, Geophys. Res. Lett., 30, L017969, doi:10.1029/2003GL017969, 2003.

Wofsy, S. C., HIPPO Science Team, and Cooperating Modellers and Satellite Teams: HIAPER Pole-to-Pole Observations (HIPPO): fine-grained, global-scale measurements of climatically important atmospheric gases and aerosols, P. R. Soc. A, 369, 2073–2086, doi:10.1098/rsta.2010.0313, 2011.

Wunch, D., Toon, G. C., Wennberg, P. O., Wofsy, S. C., Stephens, B. B., Fischer, M. L., Uchino, O., Abshire, J. B., Bernath, P., Biraud, S. C., Blavier, J.-F. L., Boone, C., Bowman, K. P., Browell, E. V., Campos, T., Connor, B. J., Daube, B. C., Deutscher, N. M., Diao, M., Elkins, J. W., Gerbig, C., Gottlieb, E., Griffith, D. W. T., Hurst, D. F., Jiménez, R., Keppel-Aleks, G., Kort, E. A., Macatangay, R., Machida, T., Matsueda, H., Moore, F., Morino, I., Park, S., Robinson, J., Roehl, C. M., Sawa, Y., Sherlock, V., Sweeney, C., Tanaka, T., and Zondlo, M. A.: Calibration of the Total Carbon Column Observing Network using aircraft profile data, Atmos. Meas. Tech., 3, 1351–1362, doi:10.5194/amt-3-1351-2010, 2010.

Wunch, D., Toon, G. C., Blavier, J.-F. L., Washenfelder, R. A., Notholt, J., Connor, B. J., Griffith, D. W. T., Sherlock, V., and Wennberg, P. O.: The total carbon column observing network, Philos. T. R. Soc. A, 369, 2087–2112, doi:10.1098/rsta.2010.0240, 2011.

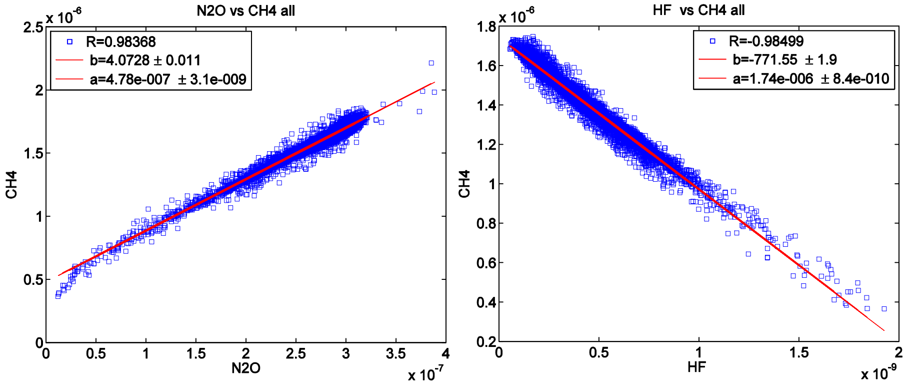

**Fig. 1.** Correlations between the stratospheric mole fractions of $N_2O$ (right) and HF (left) with $CH_4$ on a global scale. Correlation coefficient, slope and intercept are indicated in the legend.

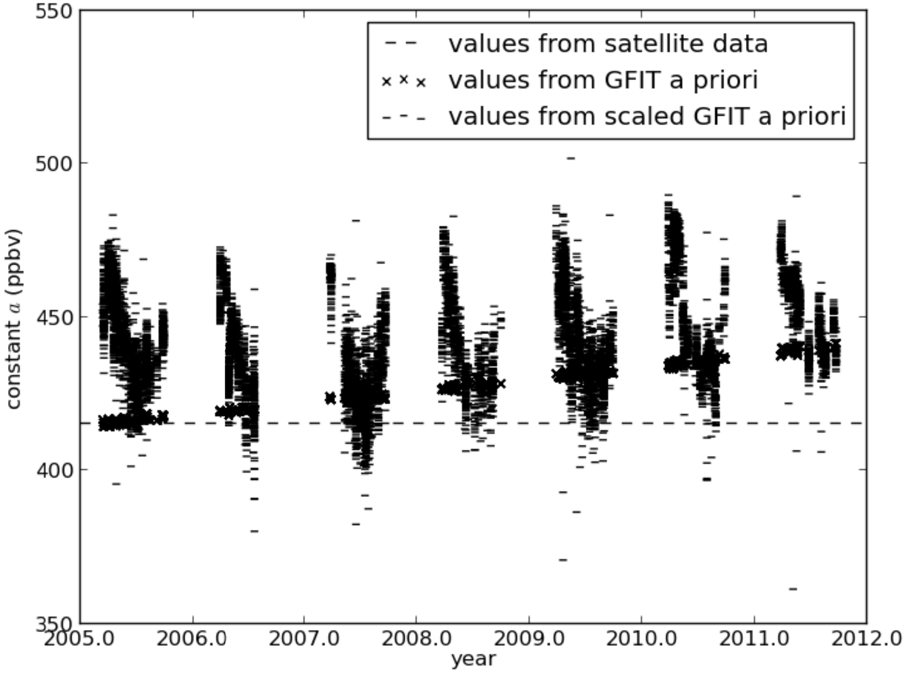

**Fig. 2.** Comparison between constant *a* derived from original and scaled GFIT a priori, ACE-FTS satellite data at Spitsbergen.

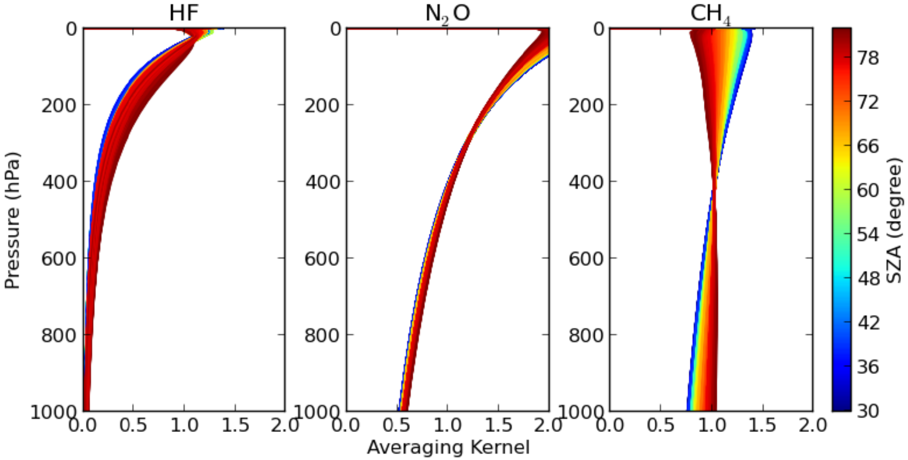

**Fig. 3.** The averaging kernels of HF, $N_2O$ and $CH_4$ at Bialystok for all spectra from 2010. The colors indicate the solar zenith angle of the corresponding measurements.

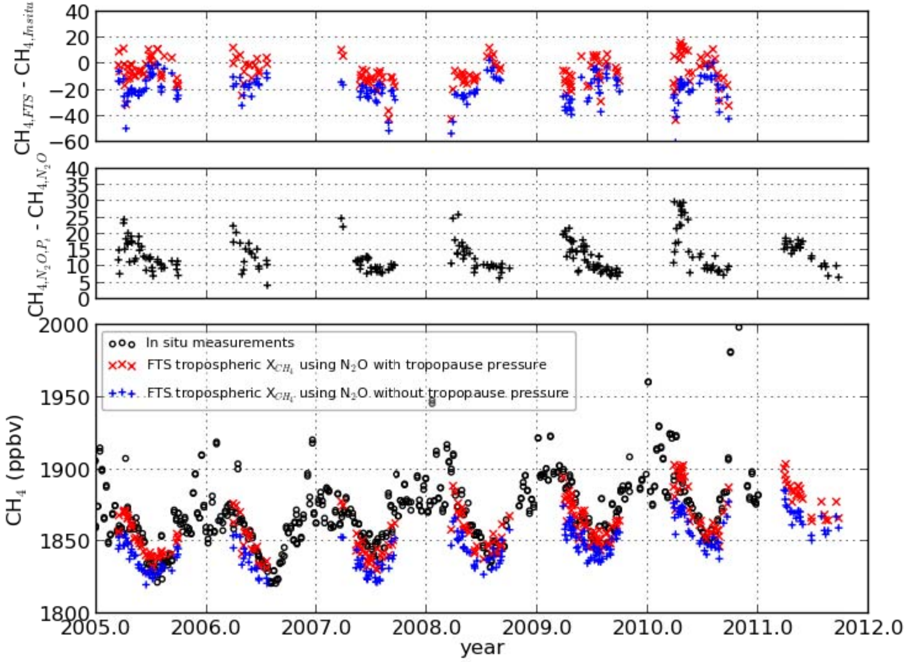

**Fig. 4.** Comparison results of two methods at Spitsbergen. The red points correspond to the tropospheric column-averaged $CH_4$ mole fraction derived from $N_2O$ and explicitly using tropopause pressure, the blue to those derived from $N_2O$ and implicitly using tropopause pressure and the open circles are in situ $CH_4$ data measured at Zeppelin mountain provided by NOAA (Dlugokencky et al., 2012). The upper panel shows the difference between the in situ $CH_4$ and the tropospheric column-averaged $CH_4$ mole fractions, the middle panel is the difference between results using two methods.

Title Page
Abstract | Introduction
Conclusions | References
Tables | Figures
◀| |▶
◀ ▶
Back | Close
Full Screen / Esc
Printer-friendly Version
Interactive Discussion

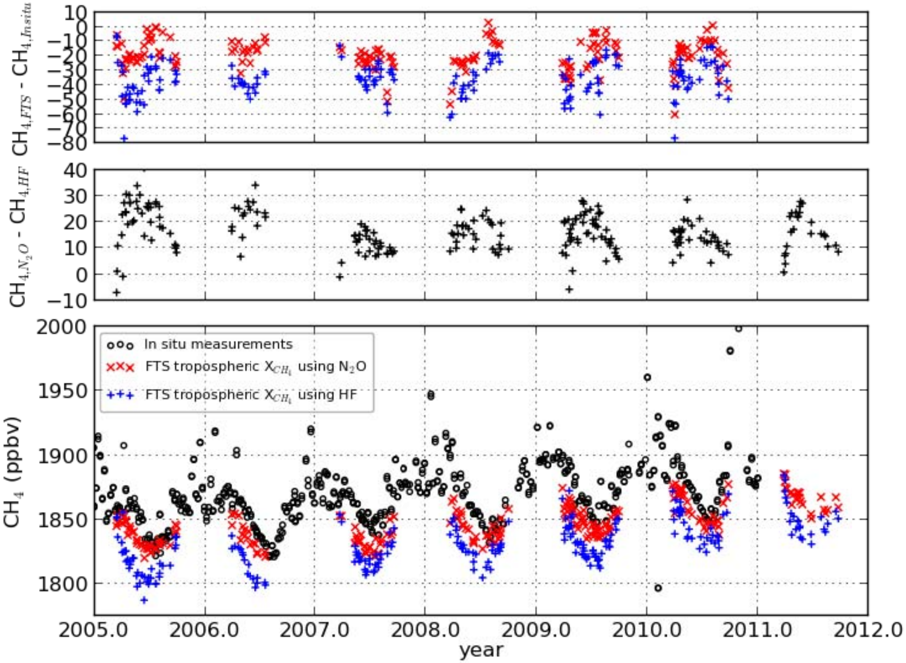

**Fig. 5.** Results at Spitsbergen, the red points correspond to the tropospheric column-averaged $CH_4$ mole fraction derived from $N_2O$, the blue to those derived using HF and the open circles are in situ $CH_4$ data measured at Zeppelin mountain. The upper panel shows the difference between the in situ and tropospheric column-averaged $CH_4$ mole fractions, the middle panel is the difference between the results using $N_2O$ and HF.

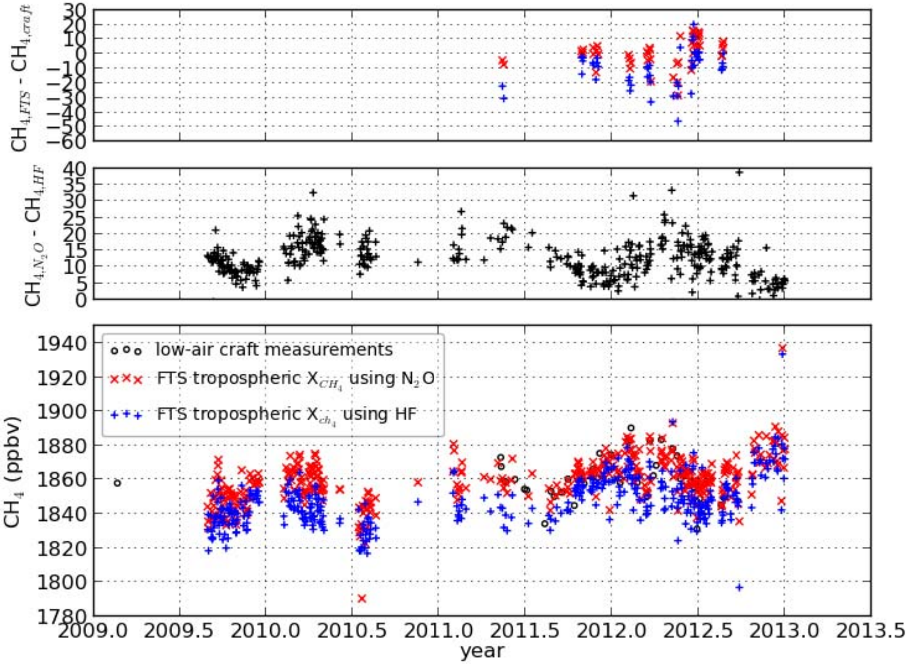

**Fig. 6.** Same as Fig. 5 except for the Orléans site and with the black points in the lower panel representing tropospheric column-averaged $CH_4$ mole fractions derived from low aircraft flights at this site.

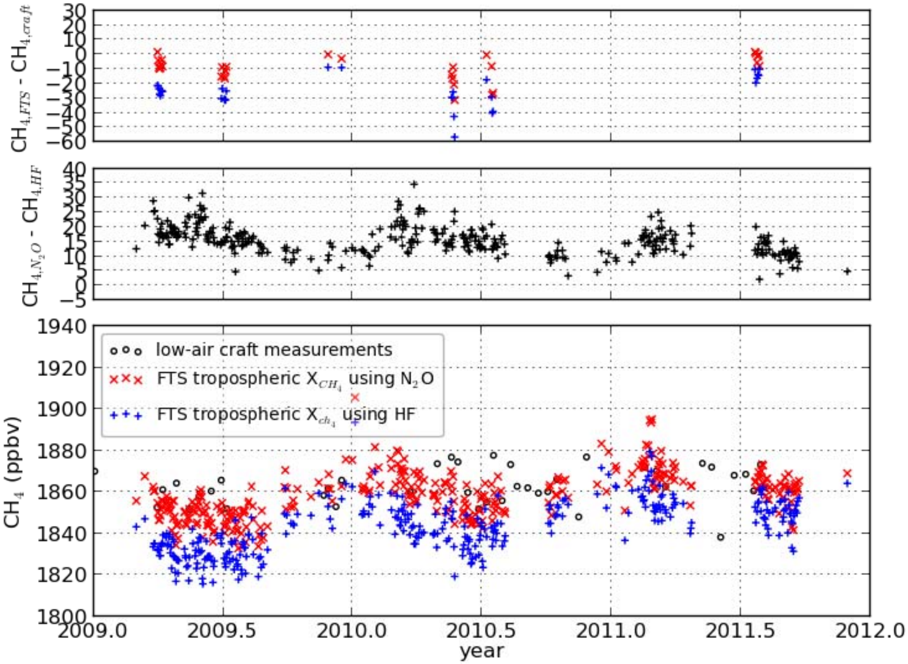

**Fig. 7.** Same with Fig. 6 except for Bialystok.

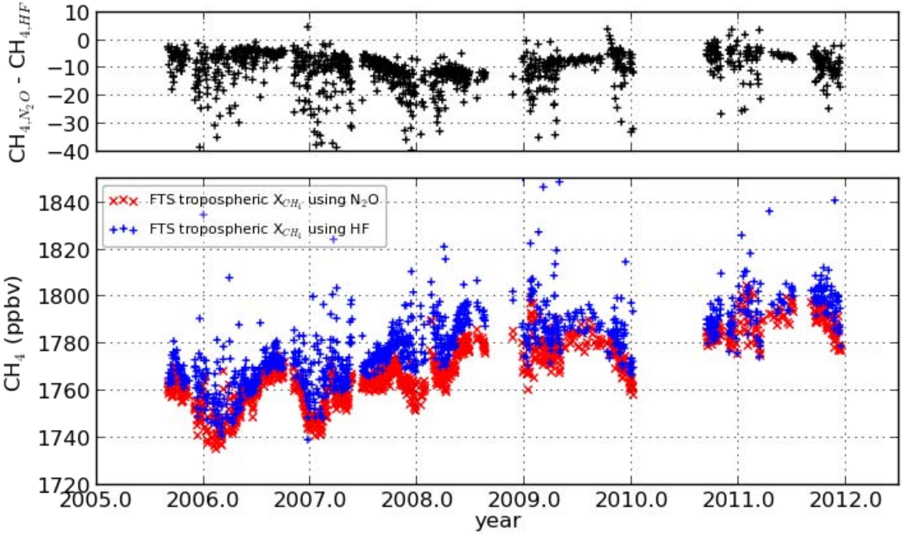

**Fig. 8.** Results at Darwin.

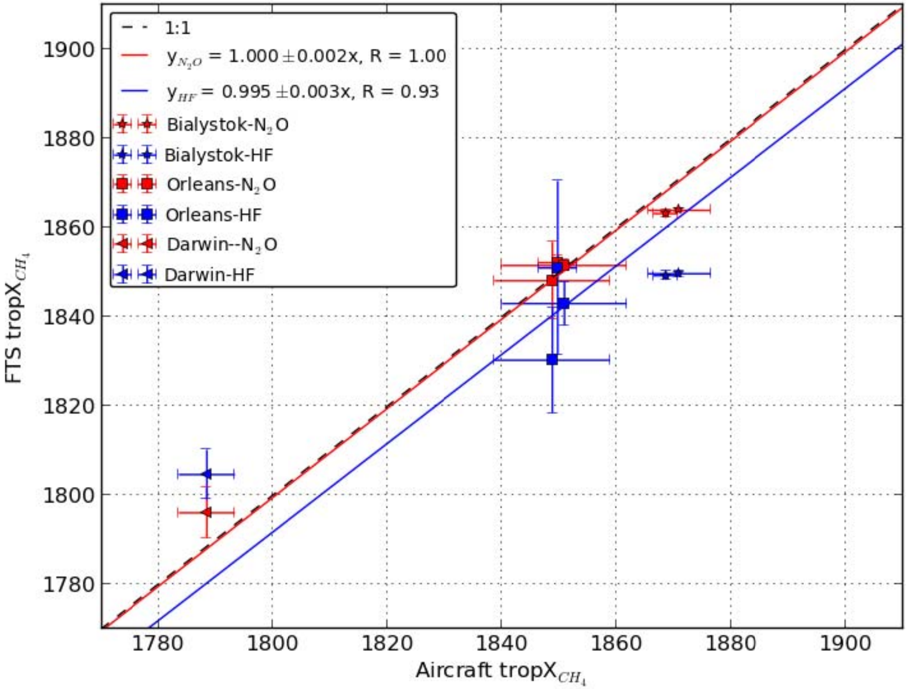

**Fig. 9.** Comparison results with aircraft data. The aircraft profiles are smoothed using GFIT averaging kernels in troposphere using Eq. (28). The FTS data are averaged through aircraft measurements periods, and the error bars of FTS data are standard deviations of these averaged data.

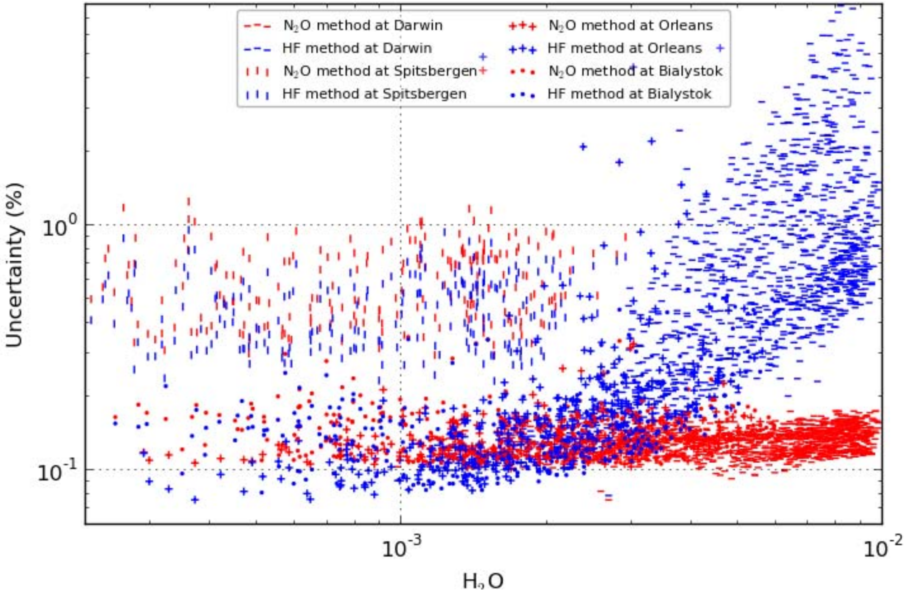

**Fig. 10.** Relative error estimation of the tropospheric column-averaged $CH_4$ mole fraction using Gaussian error propagation equation for four sites, the blue corresponds to the error for the method using HF and the red to that of method using $N_2O$.

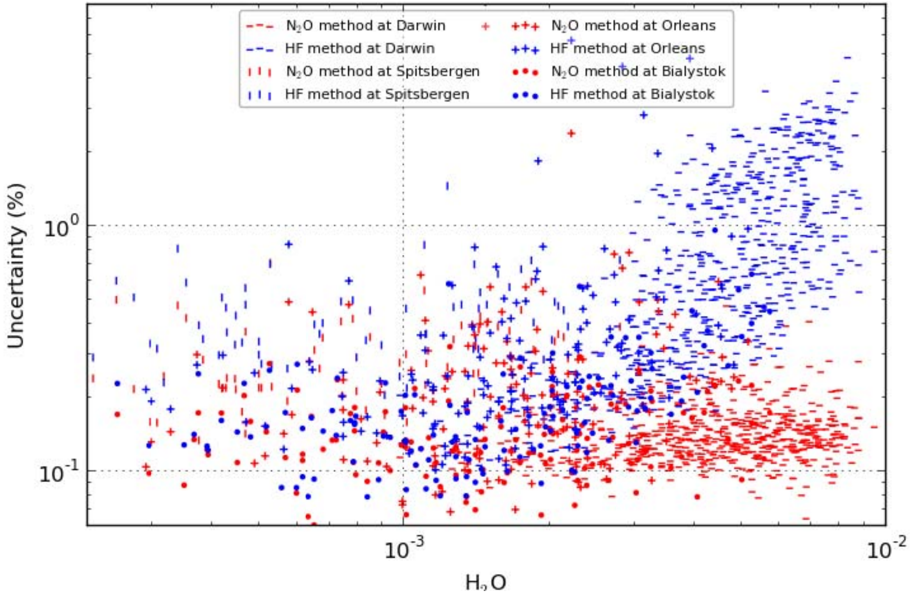

**Fig. 11.** Same as Fig. 9, except for that the relative error is estimated as the standard deviation of daily mean tropospheric $CH_4$.